ACS APPLIED MATERIALS & INTERFACES

Research Article

www.acsami.org

Surface-Mediated Extraction and Photoresponse Modulation of Bisphenol A Derivatives: A Computational Study

Swastika Banerjee[†] and Swapan K. Pati*[,†,‡]

[†]New Chemistry Unit and [‡]Theoretical Sciences Unit, Jawaharlal Nehru Center for Advanced Scientific Research, Bangalore 560064, India

Supporting Information

ABSTRACT: 2,2′-bis(4-hydroxyphenyl) propane (BPA) and its metabolites 4-methyl-2,4-bis(*p*-hydroxyphenyl)pent-2-ene (M-1) and 4-methyl-2,4-bis(4-hydroxyphenyl)pent-1-ene (M-2) are common in drinking water and hard plastics and thus pose serious health hazards. These are also known as endocrine disrupting chemicals (EDCs). In this paper, we discuss the surface-mediated adsorption mechanism and subsequent changes in the electronic structure of EDCs. This is in view of their separation from environment and possible photodecomposition. Computational investigation based on density functional theory and ab initio molecular dynamics was performed on bisphenol compounds (BPA, M-1, and M-2) as guest and affinity-based separation media as substrate. Static properties (at 0 K) and conformational dynamics upon physisorption (at T = 300 K) depict the potential of 2H-MoS_2 surface for reversible adsorption/desorption and selective isolation of these EDCs. In contrast, layered graphene supports very strong surface adsorption and assures complete removal of EDCs. In particular, optical response of the EDCs gets tuned upon surface adsorption. Hence, understanding the surface adsorption and modulation of the electronic structure would reveal possible means for extraction and photodegradation of a major class of environmental pollutants by specific choice of surface.

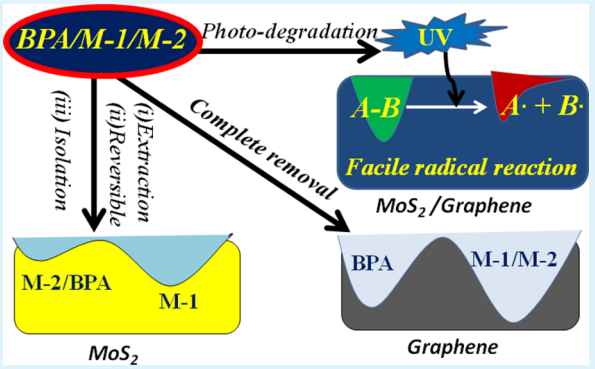

KEYWORDS: *bisphenol A, separation, removal, photo decomposition, computational, DFT, AIMD*

INTRODUCTION

Micropollutants classified as endocrine disrupting chemicals[1] (EDCs) cause severe human health risk, for example, disorder in reproductive,[2] immune,[3] hormonal,[4] and nervous systems.[5] BPA and its derivatives belong to this category of EDCs, which are commonly found in surface water, drinking water, and the commercial plastic products used in our day-to-day life. Over the last decade, there have been several efforts toward detection of these environmental pollutants.[6] There is also a deep concern for the removal of these contaminants from water.[7,8] As a matter of fact, traditional processes such as coagulation and flocculation are ineffective in this regard.[9,10] Treatment with the chemical oxidants is also limited due to the possibility of formation of even more toxic oxidation products.[11] There are few studies using reverse osmosis and nanofiltration as tools.[12] However, these techniques are economically unfeasible. In reality, both the water and wastewater treatment plants are not properly designed to remove micropollutants. In this scenario, a new technology is needed that would be abundant, efficient, and feasible. A composite of activated carbon fiber and Ce^{3+}-TiO_2 treatment has been accepted as an efficient strategy for the removal of hydrophobic micropollutants.[13,14] However, this approach is reserved for drinking water treatment. Moreover, recyclability of this material needs regenerative oxidation of absorbed BPA, creating inconvenience for practical applications. Thus, absorption−desorption kinetics is crucial to design a functional component with better synergy in terms of reusability of the material. Apart from the strategy for physical separation, detectable response upon EDC adsorption is an important factor for recognition of such micropollutants. Very recently, Huang et al. have shown that oxidation product of BPA could effectively quench the fluorescence of graphene quantum dots (GQDs).[15] The quenching of photoluminescence intensity of GQDs can give the quantitative estimate of concentration of BPA.[15] But there is irreversibility in the process, as the redox process driving the quenching cannot be recyclable. We seek two-dimensional (2D) layered materials (in contrast to QDs) with high surface area for efficient surface-adsorption.

BPA, M-1, and M-2 are termed as EDCs throughout this paper (see Figure 1). Discussions in this article are divided into two parts. In Part I, we discuss whether the EDCs can be detected and singled out with the help of the matrix. In Part II, we focus on photoinduced changes in electronic structure and photoabsorption property of EDCs in the presence of 2D matrices. The reason behind the photostability[16,17] of such

Received: June 25, 2015
Accepted: October 14, 2015
Published: October 14, 2015

ACS Publications © 2015 American Chemical Society

DOI: 10.1021/acsami.5b07949
ACS Appl. Mater. Interfaces 2015, 7, 23893−23901

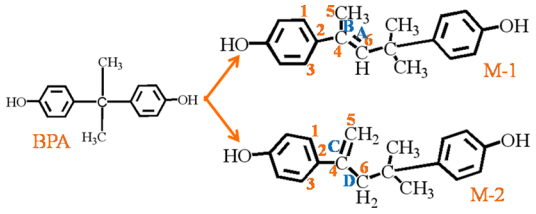

Figure 1. Molecular structures of BPA and its metabolites (M-1 and M-2) are shown. Bonds, dihedrals (DH) are assigned as A: 4−6 (M-1); B: 4−5 (M-1), C: 4−5 (M-2); D: 4−6 (M-2), DH-1:3−2−4−6 (M-1); DH-2:1−2−4−5 (M-2) (presented in Table 2).

organic molecules has also been discussed. We ask the question whether the molecular electronic states and vibration modes can be tuned using suitable matrix, which in turn would influence the optical response and, hence, possibly photodissociation of adsorbed molecules.

We selected BPA as model micropollutant because of its widespread exposure.[18] Additionally, these molecules are difficult to biodegrade.[19] BPA undergoes metabolism where two metabolites, namely, 4-methyl-2,4-bis(p-hydroxyphenyl) pent-2-ene (M-1) and 4-methyl-2,4-bis (4-hydroxyphenyl) pent-1-ene (M-2), form. The toxicity of these metabolites is even higher than the parent BPA molecule.[20] So, rapid, simple, and economically feasible removal of contaminated BPA and its derivatives in water deserves urgent attention. There are some endeavors in this regard based on photochemical,[21] electrochemical,[22] and other advanced oxidation[23,24] processes. However, here, we propose a new mechanism. Functional membrane containing few layers of pure graphene and 2H-MoS_2 were considered. Surface-mediated interaction mechanism of EDCs with two types of membranes was analyzed critically. We also quantified the interactions present in molecular self-assembly as well as molecular solvation. We select graphitic material as membrane due to its extended π delocalization. For evaluation of the adsorption capacity, we maintain a particular adsorbent concentration of ∼180 mg/g for BPA-adsorption on monolayer graphene. This critical concentration corresponds to the experimental value in previously reported literature[25] at 172 mg/g, which was among the highest values obtained in case of graphene, compared to other carbonaceous adsorbents. Considering the Brunauer−Emmett−Teller surface area of the adsorbents, the high affinity of graphene to BPA was even more obvious. Therefore, graphene was an excellent BPA absorbent in wastewater treatment. Recently, graphene−TiO_2 composite was studied for the removal and mineralization of a few pollutants.[26,27] However, MoS_2 is promising because of its low friction properties as well as robustness against dilute acids and aerial oxygen.[28] In fact MoS_2 is widely used as a solid lubricant.[29] We considered 2H-MoS_2, which is the most stable form among all the polymorphs of MoS_2.[30] In addition, being p-type material, it helps the electron-donating species to stick on the surface.[31,32] Thus, graphene and MoS_2 represent two different classes of surfaces, which were scrutinized to obtain insight into the rigidity of the bonding between substrates and the EDCs as guest molecules.

COMPUTATIONAL DETAILS

First-principles calculations are based on both the density functional theory (DFT) and ab initio molecular dynamics (AIMD) methods. DFT calculations for periodic systems were performed using the GPW formalism with Perdew−Burke−Ernzerhof (PBE) functional in the Quickstep module of the CP2K set of program.[33] We use GTH (Goedecker, Teter, and Hutter)[34] pseudopotential, and the valence electrons are handled using triple-ζ valence (TZV) basis set. The van der Waals (vdW) corrections (DFT-D2 and D3) as prescribed by Grimme[35,36] were employed for noncovalent interactions. It is noteworthy that D3 correction becomes very crucial to capture the strong adsorption feature, particularly on graphene surface. A realistic model for the specific surface adsorption of BPA, M-1, and M-2 at dilute concentration was achieved by adopting a large super cell (8 × 8) matrix (192 atoms for MoS_2; 384 atoms for bilayer graphene) compared to small adsorbed molecule (the intermolecular distances between two adsorbed molecules were kept more than 10 Å away, mimicking very dilute situation). Geometry optimizations were performed using the Broyden−Fletcher−Goldfarb−Shanno (BFGS) minimization algorithm,[37,38] with the convergence threshold of 1×10^{-4} Hartree for energy and 1×10^{-4} Hartree/Bohr for force. All the pseudopotential calculations are performed with the plane-wave cutoff of 40 Ry. The charge density cutoff was set at 480 Ry. Adsorbent/adsorbate potential energy surface directs the dynamics of adsorbed molecule. We also perform a set of calculations for monolayer graphene and MoS_2 through Quantum espresso suite of programs.[39] To maintain the concentration of ∼180 mg/g for BPA adsorption on monolayer graphene, we consider (6 × 6) supercell matrix with 141 atoms, which is applied for MoS_2 surface too. We employ the PBE functional and augmented-wave method[40] along with consideration of scalar relativistic effects for d-electrons of molybdenum. Plane-wave basis was truncated with energy cutoffs of 40 Ry in representation of wave functions, and density cutoff was fixed as 320 Ry. k-meshes (5 ×5 × 1) are used to sample Brillouin zone integration for structural optimization. We find that the CP2K results agree well with the findings through Quantum espresso. All the adsorption energy values shown in the Figure 2 in main text (for monolayer, 6 × 6 supercell),

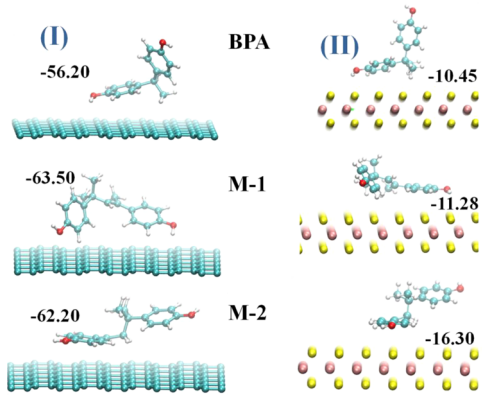

Figure 2. Equilibrium adsorption configurations with corresponding AE (kcal mol^{-1}) values for BPA (upper), M-1 (middle), and M-2 (lower) on bilayer matrices; (I) graphene, (II) MoS_2. Spheres of color white: H, cyan: C, red: O, yellow: S and pink: Mo atoms.

were calculated with Quantum espresso. For bilayer as well as at the dilute limit of adsorption (with significantly larger number of atoms, 8 × 8 supercell), we employ CP2K-based calculations. Since the modeling of real microfaceting requires the consideration of the thermal motion as well as various conformations of the adsorbed molecule on the surface, we perform AIMD simulations coupled with DFT calculations. Characterization of the dynamical physisorption on MoS_2 surface was investigated with AIMD simulation[41] at 300 K and 1 atm pressure using same package with the same level of theory. Simulations were run at 300 K using Nose-Hoover thermostat. The time step of 0.5 fs was used to integrate the equations of motion. The 5 ps trajectory was generated for analysis. For AIMD study, we freeze the matrix due to negligible geometrical perturbation in surface after molecular adsorption. Mulliken population analysis was done to assess the sharing of charges between the guest molecule and the host matrix.

DOI: 10.1021/acsami.5b07949
ACS Appl. Mater. Interfaces 2015, 7, 23893−23901

Relative stabilization (RE) of M-1/M-2 on different matrices was characterized using the following equation.

$$\mathrm{RE} = E_{\mathrm{M\text{-}1@Matrix}} - E_{\mathrm{M\text{-}2@Matrix}} \quad (1)$$

We calculate the adsorption energy (AE) of guest molecules on matrix (either graphene or MoS_2) using the following equation.

$$\mathrm{AE} = E_{\mathrm{M\text{-}1/M\text{-}2@Matrix}} - E_{\mathrm{Matrix}} - E_{\mathrm{M\text{-}1/M\text{-}2}} \quad (2)$$

where E stands for total energy (with dispersion correction) for the respective species mentioned in the subscript, and $E_{\mathrm{M\text{-}1/M\text{-}2@Matrix}}$ is the energy of the combined species of M-1 or M-2 with matrix.

Time-dependent density functional theory (TDDFT) calculations, as implemented in Gaussian 09,[42] were performed with three different levels of theories including Hartree−Fock (HF),[43] DFT with hybrid functional (B3LYP)[44,45] at B3LYP/6-311+G(d,p) level, and DFT with dispersion correction (DFT-D)[46] method at ωb97xd/6-311+G(d,p) level. Quantitative description of noncovalent interactions is highly sensitive to the choice of level of theory and computational method. For validation of the methodology and the appropriateness of the level of theory, we compared our results with the observed (see ref 47) wavelengths and relative intensities of 4,4′-methylene bisphenol (see computational details in Supporting Information, Figure S1). Wavelengths and intensities predicted with the ωb97xd/6-311+G(d, p) method in the presence of implicit solvent model (ε = 80) agree satisfactorily with experimental findings.[47] The same level of theory was used for all TDDFT calculations. The TDDFT calculations, which is impossible for periodic system, were performed only for molecule at surface-adsorbed state, since the electron transfer between surface and adsorbate molecules (BPA, M-1, and M-2) remain very weak. Thus, the geometrical changes due to dispersive interaction would give rise to changes in optical properties without the change in electron count in the molecule. Thus, it is well-accepted to consider the geometrical changes in the molecule upon surface adsorption. Hence, we performed the TD-DFT calculations on the molecule after removing the surface. Minimum-energy structures are verified by frequency calculations. Nature of the chemical bonding is discussed on the basis of natural bonding orbital analysis (NBO).[42] Natural transition orbital analysis[42] was performed for orbital interpretation of electronic excitation. Hence, orbital transformation helps to provide a description of occupied natural transition orbital paired with a single unoccupied orbital. One specific transition is weighted with the appropriate eigenvalue (1).

RESULT AND DISCUSSION

I. Surface-Mediated Interaction of Bisphenol A, M-1, and M-2. Molecular adsorption of all the three BPA compounds (see Figure 2 and Figure S4 in Supporting Information) on graphene surface occurs very strongly (AE ≈ 60 kcal mol^{-1}). According to our ab initio results, based on both the static calculation through DFT and considering the conformational dynamics through AIMD, we find the flattening of the molecule resulting in strong molecular adsorptions on the defect-free graphene surface. This result is in contrast with the adsorption on activated carbon. Additionally, enthalpy of phenol adsorption also shows weaker surface affinity and the dependence on the pore diameter of carbon nanotube, which changes from −23.9 to −18.1 kcal/mol with increasing pore diameter from 9.4 to 18.8 Å and approaches the ΔH value of −14.7 kcal/mol.[48] So, BPA shows a strong adsorption at pristine graphene surface, whereas the functionalized graphene surface shows lesser adsorption affinity. For BPA, the adsorption energy (depending on adsorption site and molecular orientation) is in the similar range as found for the phenol on Ni(111) surface[49] (0.64−0.91 eV). In both the cases, the carbon ring lies parallel to the surface at an equilibrium distance of ∼2.0 Å. The presence of surface functional group such as hydroxyl, carbonyl, or carboxylic acid in the oxidized graphene restricts the possibility for direct attachment of the BPA with graphene surface. Instead, there is favorability for adhesion of molecule on the surface through H-bonding interaction as evidenced in previous experimental study.[25] We emphasize the fact that the clean graphene surface triggers exceptionally strong adhesion and assists removal of the BPA. However, carbonaceous materials such as activated carbon, carbon nanotubes, porous carbon, and graphene oxide have large specific surface areas with abundant pore size distributions, but all of them have lesser strength for surface-adhesion.

Between two conventional models for adsorption kinetics (pseudo-first-order and pseudo-second-order) the pseudo-second-order kinetic model fits the adsorption of BPA on graphene.[25] Importantly, the pseudo-second-order model includes all the steps of adsorption including external film diffusion, adsorption, and internal particle diffusion. The magnitude (>1) of Freundlich constant supports favorable adsorption. These experimental findings[25] compare fairly well with the outcome from our molecular dynamics study. Our ab initio results support highly negative standard free-energy change. Negative standard entropy change reflects the decreased randomness at the solid−liquid interface during the adsorption of BPA on graphene for the spontaneous absorption process. Interestingly, irreversibility is associated with the strong surface affinity that supports complete removal of the BPA from environment, while pristine graphene plays the role of surface.

Decisively, strong $\pi-\pi$ stacking and C−H/O−H π interactions leads to such irreversible surface adsorption, which is evidenced from the analysis on IR stretching frequency as discussed later. EDCs consist of two terminal −OH groups as well as two aromatic rings bridged via an aliphatic spacer group. Only, the chemical nature of the aliphatic spacer group varies from one to another (BPA, M-1, and M-2; see Figure 1). Different spacer aliphatic groups for isomeric molecules (M-1/M-2) and BPA have almost equal contribution to dispersive interactions with graphene. This rules out the possibility of selective isolation of M-1 and M-2. Hence, we conjecture that the graphene layer would find application in removing the EDCs completely. Mulliken electronic charge transferred from molecule to the graphene sheet is 0.03 e upon absorption of BPA on bilayer graphene. Nature of the wave function for the conduction band minima (CBM) and valence and maxima (VBM) at the γ point supports the partial electron transfer from adsorbed molecule to the sheet (see Figure 3). Since it is difficult to do rigorous calculations to predict optical transition in a periodic system; we looked at CBM and VBM wave functions carefully. They indeed show opposite parity with the functional we used. So, the transition dipole moment would be nonzero between these two states. We find the optical band gap (1.25 eV) at the γ point upon strong absorption of BPA on bilayer graphene, arising from the coupling of electronic states to the asymmetric stretch mode. This is to say that the electronic absorption would appear in near-infrared (NIR) regime. Mobile π-electrons, induced due to strong adsorbent-surface affinity and weak electronic charge transfer from molecule to matrix, lead to a strong NIR absorption as both the states remain in the same k-point value. Thus, the response can be detectable.

In contrast to the carbonaceous surface, EDCs get adsorbed on the inorganic metal chalcogenide (MoS_2) surface through the attachment of only one terminal phenolic moiety (see

DOI: 10.1021/acsami.5b07949
ACS Appl. Mater. Interfaces 2015, 7, 23893−23901

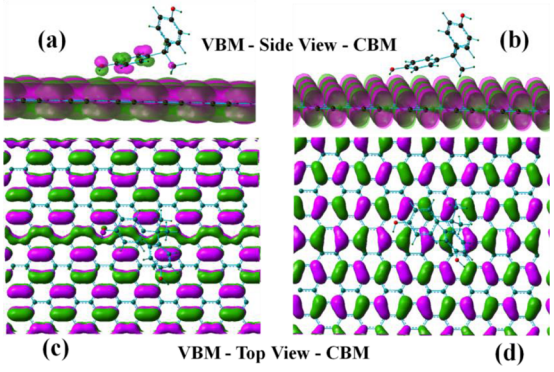

Figure 3. Γ-point VBM and CBM (frontier orbitals) for model surface topologies. (a, b) Side view of VBM and CBM for BPA@bilayer-graphene, respectively; (c, d) top view of the same. Isocontour value used for orbital plots is 0.02 e bohr^{-3}.

Figure 2 and, in Supporting Information, Figure S5). Other tail of the adsorbed molecule remains far from the surface. This confers significantly less adsorption energy (ΔE = 10−17 kcal mol^{-1}). We also performed a set of calculations and found that adsorption of BPA on 1T-MoS_2 is thermodynamically disfavorable with highly positive ΔG value. The other analogue of MoS_2, $MoSe_2$, also shows similar feature like 1T-MoS_2. Hence BPA-adsorption is specific for 2H-MoS_2 especially. Notably, structural relaxations associated with locally modified charges on adsorbed molecule results in conformational dynamics (see Figure 4). Adsorption energy for M-1 molecule

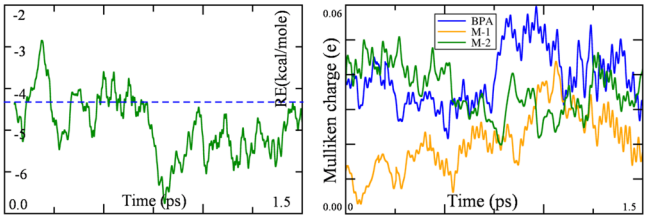

Figure 4. RE (see eq 1) vs time (left) and charge fluctuation (right) due to electronic charge transferred from molecule to the p-type surface MoS_2 triggered by conformational dynamics.

(−16.30 kcal/mol) is the highest among all three (BPA: −10.45 and M-2: −11.28 kcal/mol see Figure 2). Thus, at the optimized conformation of adsorbed state, we find M-1 becomes more stable (RE = −5.10 kcal/mol) than M-2, on MoS_2 surface. Note that, in isolated states as described in our previous work[50] and for the strong surface-absorbed state (on graphene surface) isomeric M-1/M-2 are equally stable. However, adsorption energy of water on MoS_2 surface varies (3.65−4.33 kcal/mol) depending on various possible adsorption sites. Now, the selection for adsorption on the surface appears to be in the order of M-1 > M-2 ≈ BPA ≫ H_2O. For the desorption process, the trend gets reversed (H_2O > M-2 ≈ BPA > M-1). Thus, MoS_2 surface serves the purpose of a stationary adsorbing medium analogous to the chromatographic technique and leads to a facile surface-induced isolation of EDCs. In conclusion, graphene surface is efficient due to the strong affinity but at the cost of irreversibility, whereas MoS_2 surface is facile in terms of relatively more reversible nature of adsorption as well as selective isolation.

There are two kinds of adsorbent−adsorbate interactions. One main interaction is the $\pi-\pi$ interaction between the benzene rings of BPA and the surface planes. The other is the hydrogen bonding between the oxygen-containing groups as well as C−H group (aromatic and or aliphatic) contained in BPA and respective surfaces. Importantly, structural changes in the adsorbed molecule can give rise to alteration of bond strengths and, thus, IR stretching frequencies of the specific modes participating in the interaction. To confirm the adsorption mechanism further, we performed the IR studies on the molecular structure (see Table S1 in Supporting Information) as it was in its adsorbed state over graphene and MoS_2. Such analysis, in fact, helped in identifying the presence of different interaction patterns between BPA and graphene.[25]

Emergence of new peaks at 2800−3000 and 400−1800 cm^{-1} are in accordance with the peaks from the Fourier transform IR spectrum of BPA as found experimentally, which indicates that BPA molecules were adsorbed on the surface of graphene. These new peaks originate from (i) skeletal vibrational modes (ii) aromatic C−H bonds as well as π-aromatic ring vibration in the low-energy regime. Furthermore, the stretching frequency of the O−H group in BPA gets shifted from 3700 to 3500 cm^{-1}, which can be ascribed to hydrogen bonding between hydroxyl groups in BPA and π-electronic cloud on the surface. The peak at 1640 cm^{-1} is associated with the skeletal vibration of aromatic C═C bonds, which also shifts 30 cm^{-1} and gets widened after adsorption, confirming the $\pi-\pi$ interaction[51] between the benzene rings of BPA and the graphene planes, which is less (−23 cm^{-1}) for MoS_2 surface. After comparative analysis between two different surfaces and their adsorption affinity, it is clear that $\pi-\pi$ interaction between the benzene rings of BPA and the graphene planes force strong chemisorptions as evident in the significantly higher shifting of the vibrational frequency of aromatic C═C bonds. Because of the added forces from the interaction between BPA and graphene layers, two significant changes can be expected to happen compared to pristine graphene. These are alterations in Raman spectra: (1) splitting of the 2D peak and (2) shift in the G-mode, which originates due to the control over in-plane vibration after surface adsorption.

To determine the selectivity/separation of solvated EDCs, we considered water as solvent media for water-soluble EDCs. Hence, we focus on the subtle interplay among the possible interactions such as surface−molecule, surface−solvent, solvent−molecule, and the intermolecular self-assembly. Adsorption energy of water on MoS_2 surface is in the range of 4−5 kcal/mol. This value is negligibly small compared to surface affinity of EDCs on MoS_2 Surface (∼15 kcal/mol). It also corroborates with the report on the weak interaction of water with defect-free MoS_2 surface.[52−54] Less interaction energy discards the possibility of competitive surface coverage by water that might cause limitations for accessibility of the desired molecule on the surface. In the context of molecular solvation, we find strong hydration energy for the EDCs. Typical H-bonding interactions are present between phenolic O−H and water. There is existence of H-bond varying within a range of 1.7−2.0 Å. Water molecules can act either as a bridge (H-bond distance: 1.63 and 2.10 Å) between two molecules or being associated with a single molecule by forming H-bond at ∼1.82 Å. Quantification of the adsorption energy of solvated dimer (along with 14 solvent molecules) turns out to be −31.45, −23.57, and 22.29 kcal/mol for M-1, M-2, and BPA, respectively. We find M-1 shows more surface adsorption affinity (7.88 kcal/mol) than M-2 in its solvated state too. In fact, through solvated dimer (along with 14 solvent molecules),

DOI: 10.1021/acsami.5b07949
ACS Appl. Mater. Interfaces 2015, 7, 23893−23901

we consider intermolecular (e.g., M-1···M-1), solvent−molecule, as well as solvent−solvent interactions. Considering the whole system on the surface, there appear two more interaction modes: surface−solvent and surface−-molecule, which can possibly affect the surface adsorption of the molecule in their solvated state. Also, we found the adsorption energy of a single unsolvated M-1 molecule to be ∼16 kcal/mol. Hence, dimer in the solvated state exhibits the surface affinity almost twice the value of the same for an isolated molecule. Basically, it proves that, the molecular solvation and surface adsorption are not competitive. Rather, there is a cooperative interplay between two types of interactions. In addition, surface affinity for solvent (∼4 kcal/mol) and for EDCs (∼15 kcal/mol irrespective of the state of solvation) confirms that the surface affinity of EDCs does not get affected while they are in solvated or in assembled state. However, adsorption affinity of water on the surface is much less and cannot compete with the EDCs (4−5 kcal/mol). As we want the extraction of EDCs from their water-contaminated state, we examine whether the solvation of the EDCs will hamper their sorption property on the surface. The surface-adsorption affinity (>22 kcal/mol) for all the solvated EDC dimers (BPA, M-1, and M-2) was found to be also high; we conclude that the surface adsorption does not get affected, while the EDCs are solvated. However, the solvation energy of BPA, M-1, and M-2 lies in the range from −3.5 to −3.8 kcal per water molecule. Therefore, solvation energy does not overcome of the strength of surface affinity of EDCs. Although relative affinity difference is in the order of water adsorption energy, we should point out that it is the absolute strength of the surface affinity for EDCs that eventually matter. Moreover, energetics reveal that the solvated complex gets more strongly bound to the surface when the water comes and solvates the EDCs. Thus, there is no possibility to wash out the EDCs from surface by water, which further supports the MoS_2 surface to act as an ideal matrix to extract the EDCs.

Although the effective area of contact between the EDCs and surface is less due to their nonlinear chain framework, the adsorption energy is in the order of electronvolt (see Figure 2). This needs a detailed understanding of the existence of effective surface-mediated mechanisms and charge transfer. We find the adsorption of BPA, M-1, and M-2 on both of these model surfaces (graphene and MoS_2) are dominated by the vdW interactions. This corroborates with the smaller charge-transfer interaction (see Figure 4). Combined classical charge modulation and quantum calculations indicate that dynamical behavior of the adsorbents regulates the electrostatic interaction (e transfer may vary from 0.003 to 0.06). In particular, collective behavior results in small electron transfer (∼0.03e), and a molecule diffuses laterally along the surface maximizing the interaction between polar H in molecule and S atoms on MoS_2 matrix. Through consideration of conformational dynamics of adsorbed EDCs at 300 K, we find that RE can fluctuate in the range from −3 to −7 kcal/mol (see Figure 4). Thus, conformational dynamics triggers in the interplay between electrostatic and dispersive interactions in physisorbed EDCs.

To understand the adsorbent−adsorbate interfacial interaction, zeta potential is a physical parameter quantifying the surface electrical potential of the solid particle and the stability of liquid dispersions. We find that the partial electron transfer from BPA to the sheet (∼0.03 e/BPA) results in excellent stability of graphene dispersions that originate from the mutual electrostatic repulsion among graphene sheets. This indicates the graphene sheets are negatively charged. In fact, the zeta potentials of graphene measured in aqueous solutions of BPA were observed to be negative,[25] which reached −46 mV for pH 10.0 implying sufficient mutual repulsion[55] and ensured the stability of the dispersion.

As shown in Figure 2, OH is more likely to stick with bending mode where H takes part in interaction. Importantly, OH groups are not prone to be dissociated as revealed from frequencies of the OH stretching modes (from the MD trajectories). We can account these surface-mediated interactions for broadening and shifting of the stretching mode of hydrogen-bonded hydroxyl groups. Accordingly, dispersive interaction is attributed to the interaction of surface-S lone pair with π-aromatic-ring, aromatic H atoms, polar O−H bonds, and π-cloud at spacer group. S ions also provide weak Lewis acidic (electron-acceptor) nature to the MoS_2 surface for BPA, M-1, and M-2 adsorption. These types of interactions can vary due to a subtle difference in π-cloud orientation in spacer group, which actually arises between M-1 and M-2. Thus, a difference in interaction energy is found for two isomers providing a way of isolation through surface-mediated couplings. Thus, loading the specific substances and then releasing them on the MoS_2 matrix can occur through diffusion-controlled mechanisms, without erosion of the matrix.

II. Optical Responses of Bisphenol A and Its Metabolites (M-1 and M-2). Computed absorption spectra (see Figure 5) reveal predominant UV absorption for EDCs.

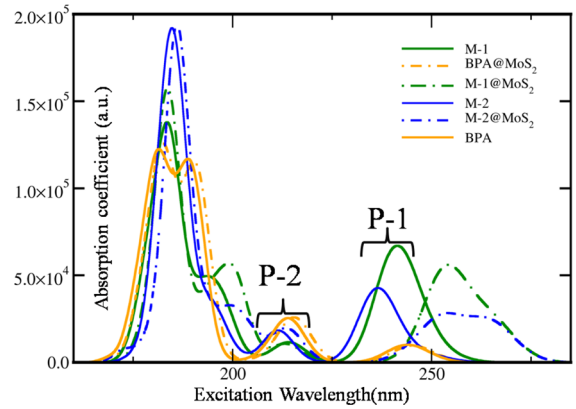

Figure 5. Computed absorption spectra of BPA, M-1, and M-2 as isolated molecules (represented by solid lines) and the matrix-adsorbed state (dotted lines) using TD-DFT corresponding two lowest absorption maxima (λ_{max}) values (P-1 and P-2) are given in Table 1.

Absorption maxima get slightly shifted ($\Delta\lambda_{max} \approx 2$ nm) by changing the dielectric constant of solvent media, that is, the nature of solvent molecule's coordination mode (see Table 1). So, probing the solvent dielectric media and structural identification of EDCs are insensible through direct investigation of the absorption spectra in different solvent media.

To understand the aspect of photodegradability of such EDCs, we focus on their photoresponse and subsequent chemical changes. We search for two major aspects upon illumination: whether (i) irreversible change in molecular shape happens or not; (ii) any site or bond becomes prone to the radical reaction or fragmentation. The natural transition orbital (NTO) shows the orbital involved in optical transition (see Figure 6). Two lowest-energy intense absorptions appear to be π to π^*. For the lowest-energy excitation, the final state turns

DOI: 10.1021/acsami.5b07949
ACS Appl. Mater. Interfaces 2015, 7, 23893−23901

Table 1. Prominent Absorption Peaks (lower energy) for M-1 and M-2, Computed Using TDDFT/ωb97xd/6-311+G(d, p)[a]

solvent environment	absorption wavelength (peaks at nm)		
	BPA	M-1	M-2
gas phase (ε = 46.7)	214, 242, 245	216, 244, 248, 256	212, 230, 244, 249
DMSO (ε = 46.7)	215, 243, 246	216, 246, 248, 256	213, 234, 244, 250
water (ε = 80)	214, 242, 245	214, 240, 245, 253	211, 236, 242, 250
explicit solvation	212, 237, 240	211, 234, 240, 248	208, 233, 237, 246

[a]Different dielectric constant of the medium (implicit solvent model) as well as explicit solvent model (four H_2O molecules are coordinated to terminal O−H bonds) show different spectral features.

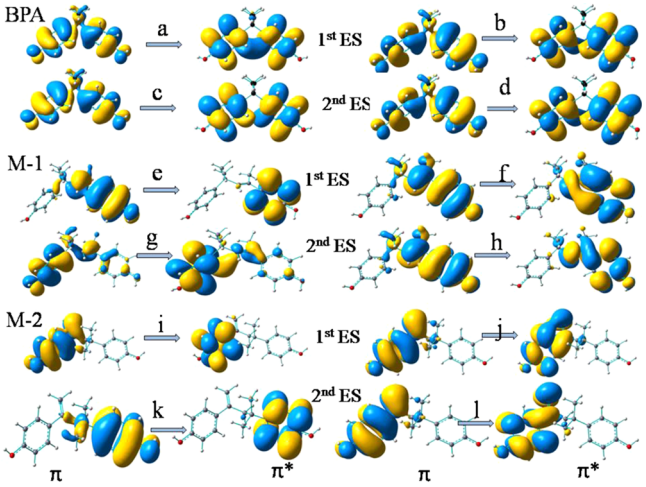

Figure 6. Dominant natural transition orbital pairs for the first two excited singlet states of BPA, M-1/M-2, and BPA/M-1/M-2@MoS_2 are given. Initial state is on the left; the final state is on the right. Associated eigenvalues are (a) 0.6057, (b) 0.5889, (c) 0.4896, (d) 0.5065, (e) 0.8604, (f) 0.9195, (g) 0.7475, (h) 9034 (i) 0.8399, (j) 0.9367, (k) 0.8408, (l) 0.8679.

out to be an antibonding orbital, the predominant contribution to which comes from C═C in the spacer group as well as aromatic ring. So, optical transition reduces the bond orders of the C═C in both the terminal aromatic rings and middle spacer part, which is common for π-delocalized systems. Interestingly, the second-lowest optical transitions are also shown to be aromatic-H assisted π-to-π* transition. Rotation of the aromatic ring about C−C (C4−C5 and C4−C6 for M-1 and M-2, respectively) bond is found to separate the charges in atoms to minimize the electron−electron repulsion. In case of M-1 and M-2, internal electron transfer occurs, where π-electrons get transferred from middle aliphatic moiety to terminal aromatic groups. Optimum bond distances lengthen by 0.07 Å for first (λ_{ex} = 249 nm; 244 nm found as shoulder in Figure 4) two lowest excitation, whereas lengthening of 0.05 Å occurs with the third excitation (λ_{ex} = 230 nm). Moreover, from NBO analysis we confirm that the bond length alterations (see Table 2) upon illumination become significant for M-1 and M-2 but not for BPA. So, spacer aliphatic moiety (absent in BPA) plays an important role in photochemistry of bisphenol compounds. Importantly, partial equalization of consecutive single and double bonds occurs in M-1 and M-2 through electronic redistribution. The middle spacer group in between two terminal phenyl groups tends to align in different plane

Table 2. Bond Orders ("Wiberg bond index") of Specific Bonds (A, B, C, D) for M-1 and M-2 (as shown in Figure 1) in Ground State (GS) and Optically Excited (1st and 2nd) States (ES)

	bond order					
	M-1			M-2		
state	A	B	DH-1	C	D	DH-2
GS	1.828	1.025	40.63	2.120	1.012	−42.11
ES-1	1.715	1.034	9.72	1.766	1.019	−7.35
ES-2	1.713	1.027	13.29	1.316	1.011	−6.40

(see the dihedral angle changes in Table 2). M-1 exhibits the most significant geometric rearrangements followed by M-2 and BPA. Basically, π-electron in aliphatic spacer group contributes to such changes, and because of its absence BPA exhibits the less structural distortion (less electronic redistribution throughout the molecular framework due to optical transition). Thus, optical excitation creates concomitant shape rearrangements of different extents for different EDCs. However, such geometrical changes upon photoexcitation are reversible. This was confirmed by our AIMD study. We find that, within ∼500 fs, the photoexcited state conformation of M-1 relaxed back to the ground-state configuration. Thus, the photodecomposition due to the irreversible shape changes in the EDCs (BPA, M-1, and M-2) becomes impossible. However, in the surface-absorbed state, terminal aromatic ring becomes electron-rich and susceptible for electrophilic attack (e.g., by $OH^{\bullet}$; see nature of the orbital in Figure 7D,E). This would give

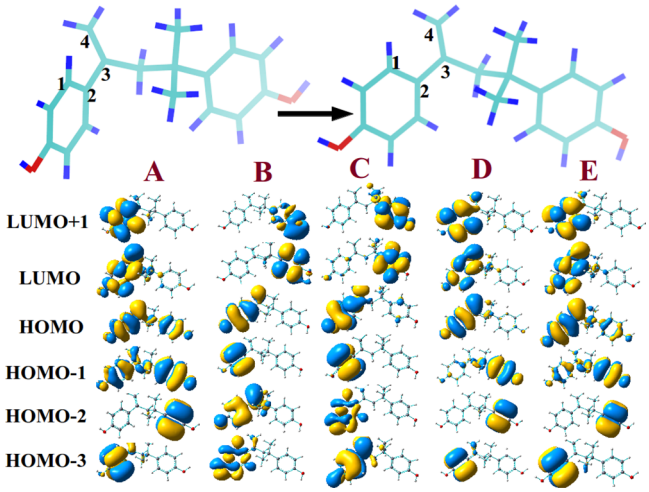

Figure 7. Molecular orbital representation of M-2 in the presence of various perturbing influences: (A) ground state; (B) directional static electric field (0.018 au); (C) uniform static electric field (0.018 au); (D) optically excited state (1st); (E) adsorbed (physisorption) on MoS_2 matrix.

rise to the decomposition of aromatic ring and, hence, might facilitate photodecomposition. So, a possibility for surface-assisted photodegradation was found, which is in accordance with our molecular orbital analysis.

Thus, the preceding discussion reveals that BPA metabolites (M-1and M-2) are photoresponsive, but in the UV absorption region. However, shifting of absorption spectral range from UV to visible is desirable for efficient solar-energy absorption. We find EDCs can also absorb much lower wavelength ($\Delta\lambda \approx +50$ nm) solar radiation (see Figure 5 and Table S2) after surface

DOI: 10.1021/acsami.5b07949
ACS Appl. Mater. Interfaces 2015, 7, 23893−23901

Table 3. A, B, C, D, E Dictates Optimized State in Presence and Absence of Various External Perturbing Influences As Described in Figure 6[a]

structural parameters	A(G)	A(W)	B	C	D	E(MO)	E(GR)
			M-1				
length (Å)	11.49	11.46	12.14	12.15	11.27	11.77	12.03
A (Å)	1.35	1.35	1.37	1.36	1.41	1.35	1.35
B (Å)	1.51	1.51	1.52	1.52	1.52	1.52	1.52
DH-1 (deg)	40.63	39.92	26.18	−33.06	9.72	28.59	30.26
			M-2				
length (Å)	13.07	13.17	12.69	12.22	13.25	13.11	12.73
C (Å)	1.34	1.34	1.35	1.37	1.41	1.35	1.35
D (Å)	1.52	1.52	1.53	1.55	1.43	1.51	1.52
DH-2 (deg)	−42.11	−40.56	−26.80	34.58	−7.35	−20.16	9.06

[a]Within parentheses: A(G): gasphase; A(W): water dielectric medium; B: directional static electric field (0.018 a.u.); C: uniform static electric field (0.018 a.u.); D: Optically excited state (1st); E(MO): adsorbed on MoS_2 surface; E(GR): adsorbed on graphene surface.

absorption. This is attributed to the extended delocalization through terminal aromatic and aliphatic moiety in spacer group. In fact, adsorptive surfaces also help to gather EDCs, as discussed in Part I, then drive the photoexcitation/degradation processes. Hence, we propose the utilization of surface coating on photocatalytic surfaces (such as TiO_2) with graphene and MoS_2. Because of the specific surface (on graphene, MoS_2) adsorptions of M-1 and M-2, red shifting of low-energy absorption peaks (see Figure 5 and Table S2) occurs. Higher-energy (lower λ) peaks do not get much affected in the presence of the matrix. But, lowest-energy peaks get broadened and split into two (see Figure 5 and Figure S2 in Supporting Information) due to coupling between the surface and adsorbed molecule.

Indeed, the spectral shift is attributed to the perturbing influence of the matrix on π-electronic cloud in transition orbital (see Figure 6 and Figure S3 in Supporting Information). As a result, surface induces conformational changes and subsequent electronic redistribution of the π-electronic cloud in the spacer group of adsorbed molecule in its excited state. Particularly interesting is the π-electronic cloud in spacer group, which dictates different extent of stabilization to each of the states involved in transition. In fact, this has great importance in case of surface-induced spectral shifting. This understanding decisively brings out the possibilities for alteration of absorption-spectral region of EDCs through appropriate choice of matrices.

Next, we look for the basic difference in the impact of electric polarization and optical pulses on each of these molecules of interest. In presence of electric polarization, M-1 and M-2 undergo a conformational change without major changes in bond order (at less electric field strength <0.26 V/Å).[50] Switchable stereocontrol of M-2 associated with O−H bond reorientation was elaborated in our earlier study.[50] However, the threshold value of uniform electric field was found to be 0.93 V/Å to induce bond order alteration. This static electric field strength creates redistribution of electron density and intramolecular charge transfer. In contrast, when exposed to specific wavelengths of light (see Table 2), optical field distorts the ground-state (GS) optimized geometry by elongating C═C and shortening the C−C bond, hence, resulting in a structural transformation (see Table 2 and Figure 7) to arrive at the other degenerate ground state.

In this section, we discuss the influences of various perturbing influences to utilize them as a tool for removal and photodegradation of EDCs. The changes in electron delocalization pattern are also reflected in their structural parameters (see Table 3). Hence, the perturbing efficiency, reflected through several structural parameters, is dependent on the directional feature of the electric field. We find that there are clearly visible changes, including large shifts of charge density from one end of the molecule to the other due to both the optical and electric field-induced perturbation. But, the estimation of the electric field strength required for such changes is quite high (~1.0 V/Å). However, optimization of the optically excited state would give rise to similar structural perturbation, which can be achieved upon irradiation with UV radiation (250 nm), which is less abundant in solar spectrum. These drawbacks associated with electric field and optical excitation drove us to search for other options. We find capturing of EDCs can easily be achieved by surface adsorption, but the electronic states (highest occupied molecular orbital (HOMO) and lowest unoccupied molecular orbital in particular) do not change drastically upon surface adsorption. Only a slight modification in the orbital representations reflects the changes in molecular electronic structure, which is governed by little conformational changes. Actually, there is no signature of catastrophic structural breakdown as evident from the structural parameters in Table 3. Thus, surface adsorption appears to be perfectly reversible in nature (for MoS_2 as substrate). Importantly, as we always look for reversibility to achieve a recyclable isolation process, the perturbation should not be very strong as found in case of graphene surface. Hence, MoS_2 surface proves its superiority.

We assessed the reactivity of the adsorbed species based on the electronic structural feature of the molecule in its isolated and surface-adsorbed states. To be more precise, we looked to see whether the orbital representation changes and whether the changes can give rise to reactivity in the adsorbed species. What we find is as follows, irrespective of the state, whether it is surface-adsorbed or an isolated molecule, two terminal rings possess more electron density, which indicates that the terminal aromatic rings will be prone to electrophilic attack. In presence of surface, the process can be facilitated due to easy exposure of the reactive sites to the electrophile. Electron density redistribution throughout molecular structural framework occurs due to surface adsorption. For isolated state, two terminal aromatic rings possess homogeneous electron density, whereas inhomogeneity occurs after surface adsorption. As a result, one terminal ring is found to have more electron density than the other. Moreover, relative reduction in the electron density for occupied states (HOMO−1 and HOMO) in

DOI: 10.1021/acsami.5b07949
ACS Appl. Mater. Interfaces 2015, 7, 23893−23901

surface-adsorbed state reflects that molecules can support the electron injection (nucleophilic attack) too. Thus, surface adsorption facilitates molecular accumulation on the surface and creates appropriate sites for both the electrophilic and nucleophilic attacks, which may lead to structural fragmentation.

CONCLUSION

In summary, MoS_2 surface exhibits optimum surface−molecule affinity and hence is perfect for reversible extraction of EDCs from environment. Surface adsorption is dominated by dispersive interaction, which is sensitive to the nature of the spacer aliphatic group of EDCs. Thus, different EDCs, on the basis of varying spacer groups, can be isolated selectively. The charge transfer from EDCs to the surface is negligibly small and gets tuned (from 0.005 to 0.06 e) by conformational dynamics. However, graphene bilayer matrix results in very strong adsorption of EDCs with a detectable response at NIR regime. Associated results are of value in designing graphene surface for complete removal and graphene−TiO_2 composite for degradation of bisphenol-based EDCs. The separation efficacy for both the matrices (graphene and MoS_2) is not affected at the solvated state of the molecules. These microscopic details demonstrate the superiority of the membrane in cleaning water by affinity-based separation of such pollutants. In the context of the optical responses of EDCs, we find that only dielectric constant of the medium cannot confer significant changes in spectral feature. Interestingly, carbonaceous substrate (bilayer graphene) and metal dichalcogenide (MoS_2) as matrices cause significant red-shifting (∼40 nm) of absorption spectra, covering a broad spectral range. Because of photoexcitation, internal electron transfer occurs from π-system to C═C antibond, decreasing the bond order. Prominently, terminal phenyl rings of EDCs become prone to undergo radical reaction at surface-absorbed (on MoS_2) state. Thus, surface-assisted photodegradation of BPA metabolites seems to be appropriate due to the bond-dissociative internal electron-transfer mechanism, triggered by optical transition. We conjecture that surface-assisted degradation of the EDCs in the presence of external perturbation is very much plausible.

ASSOCIATED CONTENT

Supporting Information

Computation details, validation of methodology, table containing IR stretching frequency data, optical absorption spectra, natural transition orbital involved in transition, equilibrium adsorption configurations. This information if available free of charge via the Internet at http://pubs.acs.org/. The Supporting Information is available free of charge on the ACS Publications website at DOI: 10.1021/acsami.5b07949.

(PDF)

AUTHOR INFORMATION

Corresponding Author

*E-mail: swapan.jnc@gmail.com.

Notes

The authors declare no competing financial interest.

ACKNOWLEDGMENTS

S.B. is grateful to CSIR (Government of India) for a senior research fellowship, and S.K.P. is grateful to DST (Government of India) for a research grant.

REFERENCES

(1) Hall, J. M.; McDonnell, D. P.; Korach, K. S. Allosteric Regulation of Estrogen Receptor Structure, Function, and Coactivator Recruitment by Different Estrogen Response Elements. *Mol. Endocrinol.* **2002**, *16*, 469−486.

(2) Atkinson, A.; Roy, D. In Vivo DNA Adduct Formation by Bisphenol A. *Environ. Mol. Mutagen.* **1995**, *26*, 60−66.

(3) Casanova-Nakayama, A.; Wenger, M.; Burki, R.; Eppler, E.; Krasnov, A.; Segner, H. Endocrine Disrupting Compounds: Can They Target the Immune System of Fish? *Mar. Pollut. Bull.* **2011**, *63*, 412−416.

(4) Ben-Jonathan, N.; Steinmetz, R. Xenoestrogens: The Emerging Story of Bisphenol A. *Trends Endocrinol. Metab.* **1998**, *9*, 124−128.

(5) Eriksson, P.; Jakobsson, E.; Fredriksson, A. Developmental Neurotoxicity of Brominated Flame-Retardants, Polybrominated Diphenyl Ethers and Tetrabromo-Bis-Phenol A. *Organohalogen Compd.* **1998**, *35*, 375.

(6) Huerta-Fontela, M.; Galceran, M. T.; Ventura, F. Occurrence and Removal of Pharmaceuticals and Hormones Through Drinking Water Treatment. *Water Res.* **2011**, *45*, 1432−1442.

(7) Klavarioti, M.; Mantzavinos, D.; Kassinos, D. Removal of Residual Pharmaceuticals from Aqueous Systems by Advanced Oxidation Processes. *Environ. Int.* **2009**, *35*, 402−417.

(8) Matilainen, A.; Vepsäläinen, M.; Sillanpää, M. Natural Organic Matter Removal by Coagulation During Drinking Water Treatment: A Review. *Adv. Colloid Interface Sci.* **2010**, *159*, 189−197.

(9) Vieno, N.; Tuhkanen, T.; Kronberg, L. Removal of Pharmaceuticals in Drinking Water Treatment: Effect of Chemical Coagulation. *Environ. Technol.* **2006**, *27*, 183−192.

(10) Suarez, S.; Lema, J. M.; Omil, F. Pre-Treatment of Hospital Wastewater by Coagulation-Flocculation and Flotation. *Bioresour. Technol.* **2009**, *100*, 2138−2146.

(11) Adams, C. D.; Randtke, S. J. Ozonation Byproducts of Atrazine in Synthetic and Natural Waters. *Environ. Sci. Technol.* **1992**, *26*, 2218−2227.

(12) Radjenovic, J.; Petrovic, M.; Ventura, F.; Barcelo, D. Rejection of Pharmaceuticals in Nanofiltration and Reverse Osmosis Membrane Drinking Water Treatment. *Water Res.* **2008**, *42*, 3601−3610.

(13) Matilainen, A.; Vieno, N.; Tuhkanen, T. Efficiency of the Activated Carbon Filtration in the Natural Organic Matter Removal. *Environ. Int.* **2006**, *32*, 324−331.

(14) Liu, L.; Zheng, G.; Yang, F. Adsorptive Removal and Oxidation of Organic Pollutants from Water Using a Novel Membrane. *Chem. Eng. J.* **2010**, *156*, 553−556.

(15) Huang, H.; Feng, Z.; Li, Y.; Liu, Z.; Zhang, L.; Ma, Y.; Tong, J. Highly Sensitive Detection of Bisphenol A in Food Packaging Based on Graphene Quantum Dots and Peroxidase. *Anal. Methods* **2015**, *7*, 2928−2935.

(16) Nomiyama, K.; Tanizaki, T.; Koga, T.; Arizono, K.; Shinohara, R. Oxidative Degradation of BPA Using Tio2 in Water, and Transition of Estrogenic Activity in the Degradation Pathways. *Arch. Environ. Contam. Toxicol.* **2007**, *52*, 8−15.

(17) Guo, C.; Ge, M.; Liu, L.; Gao, G.; Feng, Y.; Wang, Y. Directed Synthesis of Mesoporous TiO2Microspheres: Catalysts and Their Photocatalysis for Bisphenol A Degradation. *Environ. Sci. Technol.* **2010**, *44*, 419−425.

(18) Krishnan, A. V.; Stathis, P.; Permuth, S. F.; Tokes, L.; Feldman, D. Bisphenol-A: An Estrogenic Substance is Released from Polycarbonate Flasks During Autoclaving. *Endocrinology* **1993**, *132*, 2279−2286.

(19) Staples, C. A.; Dome, P. B.; Klecka, G. M.; Oblock, S. T.; Harris, L. R. A Review of the Environ. Fate, Effects, and Exposures of Bisphenol A. *Chemosphere* **1998**, *36*, 2149−2173.

(20) Yoshihara, S. i.; Mizutare, T.; Makishima, M.; Suzuki, N.; Fujimoto, N.; Igarashi, K.; Ohta, S. Potent Estrogenic Metabolites of Bisphenol A and Bisphenol B Formed by Rat Liver S9 Fraction: Their Structures and Estrogenic Potency. *Toxicol. Sci.* **2004**, *78*, 50−59.

(21) Ohko, Y.; Ando, I.; Niwa, C.; Tatsuma, T.; Yamamura, T.; Nakashima, T.; Kubota, Y.; Fujishima, A. Degradation of Bisphenol A

DOI: 10.1021/acsami.5b07949
ACS Appl. Mater. Interfaces 2015, 7, 23893−23901

in Water by TiO2 Photocatalyst. *Environ. Sci. Technol.* **2001**, *35*, 2365−2368.
(22) Xie, Y.-B.; Li, X.-Z. Degradation of Bisphenol A in Aqueous Solution by H_2O_2-Assisted Photoelectrocatalytic Oxidation. *J. Hazard. Mater.* **2006**, *138*, 526−533.
(23) Horikoshi, S.; Kajitani, M.; Serpone, N. The Microwave-/Photo-Assisted Degradation of Bisphenol-A in Aqueous TiO 2 Dispersions Revisited: Re-Assessment of the Microwave Non-Thermal Effect. *J. Photochem. Photobiol., A* **2007**, *188*, 1−4.
(24) Tanaka, S.; Nakata, Y.; Kuramitz, H.; Kawasaki, M. Electrochemical Decomposition of Bisphenol A and Nonylphenol Using a Pt/Ti Electrode. *Chem. Lett.* **1999**, *28*, 943−944.
(25) Xu, J.; Wang, L.; Zhu, Y. Decontamination of Bisphenol A from Aqueous Solution by Graphene Adsorption. *Langmuir* **2012**, *28*, 8418−8425.
(26) Liu, C.; Teng, Y.; Liu, R.; Luo, S.; Tang, Y.; Chen, L.; Cai, Q. Fabrication of Graphene Films on TiO 2 Nanotube Arrays for Photocatalytic Application. *Carbon* **2011**, *49*, 5312−5320.
(27) Wang, W.-S.; Wang, D.-H.; Qu, W.-G.; Lu, L.-Q.; Xu, A.-W. Large Ultrathin Anatase TiO2 Nanosheets with Exposed {001} Facets on Graphene for Enhanced Visible Light Photocatalytic Activity. *J. Phys. Chem. C* **2012**, *116*, 19893−19901.
(28) Liu, N.; Kim, P.; Kim, J. H.; Ye, J. H.; Kim, S.; Lee, C. J. Large-Area Atomically Thin MoS2 Nanosheets Prepared Using Electrochemical Exfoliation. *ACS Nano* **2014**, *8*, 6902−6910.
(29) Savan, A.; Pfluger, E.; Voumard, P.; Schroer, A.; Simmonds, M. Modern Solid Lubrication: Recent Developments and Applications of MoS2. *Lubr. Sci.* **2000**, *12*, 185−203.
(30) Hershfinkel, M.; Gheber, L. A.; Volterra, V.; Hutchison, J. L.; Margulis, L.; Tenne, R. Nested Polyhedra of MX2 (M= W, Mo; X= S, Se) Probed by High-Resolution Electron Microscopy and Scanning Tunneling Microscopy. *J. Am. Chem. Soc.* **1994**, *116*, 1914−1917.
(31) Rao, C. N. R.; Maitra, U.; Waghmare, U. V. Extraordinary Attributes of 2-Dimensional MoS 2 Nanosheets. *Chem. Phys. Lett.* **2014**, *609*, 172−183.
(32) Rao, C. N. R.; Gopalakrishnan, K.; Maitra, U. Comparative Study of Potential Applications of Graphene, MoS2, and Other Two-Dimensional Materials in Energy Devices, Sensors, and Related Areas. *ACS Appl. Mater. Interfaces* **2015**, *7*, 7809−7832.
(33) Perdew, J. P.; Burke, K.; Ernzerhof, M. Generalized Gradient Approximation Made Simple. *Phys. Rev. Lett.* **1996**, *77*, 3865.
(34) Elstner, M.; Porezag, D.; Jungnickel, G.; Elsner, J.; Haugk, M.; Frauenheim, T.; Suhai, S.; Seifert, G. Self-Consistent-Charge Density-Functional Tight-Binding Method for Simulations of Complex Materials Properties. *Phys. Rev. B: Condens. Matter Mater. Phys.* **1998**, *58*, 7260−7268.
(35) Grimme, S.; Ehrlich, S.; Goerigk, L. Effect of the Damping Function in Dispersion Corrected Density Functional Theory. *J. Comput. Chem.* **2011**, *32*, 1456−1465.
(36) Goerigk, L.; Grimme, S. A Thorough Benchmark of Density Functional Methods for General Main Group Thermochemistry, Kinetics, and Noncovalent Interactions. *Phys. Chem. Chem. Phys.* **2011**, *13*, 6670−6688.
(37) Møller, M. F. A Scaled Conjugate Gradient Algorithm for Fast Supervised Learning. *Neural Networks* **1993**, *6*, 525−533.
(38) Head, J. D.; Zerner, M. C. A Broyden-Fletcher-Goldfarb-Shanno Optimization Procedure for Molecular Geometries. *Chem. Phys. Lett.* **1985**, *122*, 264−270.
(39) Giannozzi, P.; Baroni, S.; Bonini, N.; Calandra, M.; Car, R.; Cavazzoni, C.; Ceresoli, D.; Chiarotti, G. L.; Cococcioni, M.; Dabo, I.; et al. QUANTUM ESPRESSO: A Modular and Open-Source Software Project for Quantum Simulations of Materials. *J. Phys.: Condens. Matter* **2009**, *21*, 395502.
(40) Blöchl, P. E. Projector Augmented-Wave Method. *Phys. Rev. B: Condens. Matter Mater. Phys.* **1994**, *50*, 17953.
(41) Hutter, J.; Iannuzzi, M.; Schiffmann, F.; VandeVondele, J. cp2k: Atomistic Simulations of Condensed Matter Systems. *Wiley Interdiscip. Rev. Comput. Mol. Sci.* **2014**, *4*, 15−25.
(42) Frisch, M.; Trucks, G. W.; Schlegel, H. B.; Scuseria, G. E.; Robb, M. A.; Cheeseman, J. R.; Scalmani, G.; Barone, V.; Mennucci, B.; Petersson, G. A. *Gaussian 09,* Revision A. 02; Gaussian. Inc.: Wallingford, CT, 2009; p 200.
(43) McLachlan, A. D.; Ball, M. A. Time-Dependent Hartree-Fock Theory for Molecules. *Rev. Mod. Phys.* **1964**, *36*, 844.
(44) Lee, C.; Yang, W.; Parr, R. G. Development of the Colle-Salvetti Correlation-Energy Formula into a Functional of the Electron Density. *Phys. Rev. B: Condens. Matter Mater. Phys.* **1988**, *37*, 785−789.
(45) Becke, A. D. Density-Functional Thermochemistry. III. The Role of Exact Exchange. *J. Chem. Phys.* **1993**, *98*, 5648−5652.
(46) Snook, I. K.; Per, M. C.; Seyed-Razavi, A.; Russo, S. P. Some Comments on the DFT+D Method. *Chem. Phys. Lett.* **2009**, *480*, 327−329.
(47) Watanabe, N.; Horikoshi, S.; Kawabe, H.; Sugie, Y.; Zhao, J.; Hidaka, H. Photodegradation Mechanism for Bisphenol A at the TiO 2/H 2 O Interfaces. *Chemosphere* **2003**, *52*, 851−859.
(48) Efremenko, I.; Sheintuch, M. Predicting Solute Adsorption on Activated Carbon: Phenol. *Langmuir* **2006**, *22*, 3614−3621.
(49) Delle Site, L.; Leon, S.; Kremer, K. BPA-PC on a Ni (111) Surface: The Interplay Between Adsorption Energy and Conformational Entropy for Different Chain-End Modifications. *J. Am. Chem. Soc.* **2004**, *126*, 2944−2955.
(50) Banerjee, S.; Periyasamy, G.; Pati, S. K. Formation Mechanism and Possible Stereocontrol of Bisphenol A Derivatives: A Computational Study. *J. Phys. Chem. B* **2014**, *118*, 9258−9262.
(51) Coughlin, R. W.; Ezra, F. S. Role of Surface Acidity in the Adsorption of Organic Pollutants on the Surface of Carbon. *Environ. Sci. Technol.* **1968**, *2*, 291−297.
(52) Putungan, D. B.; Kuo, J.-L. Structural and Electronic Properties of Monolayer 1T-MoS2 Phase, and Its Interaction with Water Adsorbed on Perfect, Single S-Vacated and MoS2-Unit-Vacated Surface: Density Functional Theory Calculations. *Integr. Ferroelectr.* **2014**, *156*, 93−101.
(53) Frame, F. A.; Osterloh, F. E. CdSe-MoS2: A Quantum Size-Confined Photocatalyst for Hydrogen Evolution from Water Under Visible Light. *J. Phys. Chem. C* **2010**, *114*, 10628−10633.
(54) Li, Y.; Wang, H.; Xie, L.; Liang, Y.; Hong, G.; Dai, H. MoS2 Nanoparticles Grown on Graphene: An Advanced Catalyst for the Hydrogen Evolution Reaction. *J. Am. Chem. Soc.* **2011**, *133*, 7296−7299.
(55) Hunter, R. J. *Zeta Potential in Colloid Science: Principles and Applications;* Academic Press: London, England, 1981.

DOI: 10.1021/acsami.5b07949
ACS Appl. Mater. Interfaces 2015, 7, 23893−23901